AIAA JOURNAL
Vol. 38, No. 12, December 2000

High-Enthalpy Expansion Tube Experiments with Gas Injection

Akihiro Sasoh*
Tohoku University, Sendai 980-8577, Japan
and
Richard G. Morgan,† Bradley N. Littleton,‡ Timothy J. McIntyre,§ and Alexis I. Bishop‡
University of Queensland, Brisbane, Queensland 4072, Australia

An experimental study was conducted to develop a system for superorbital high-enthalpy flow simulation with gas injection. The expansion tube X-2 was used as the base facility. The synchronization of the gas injection to the expansion tube operation and the effect of the gas injection on the high-enthalpy flow generation performance are carefully discussed. When hydrogen was injected, the performance of the acceleration tube operation was not degraded, whereas with nitrogen injection the shock speed was significantly decreased. Hypersonic shock layers with gas injection were visualized by the schlieren method. This system is expected to be used as a tool to simulate a hypersonic shock layer with ablation for a reentry capsule.

I. Introduction

WITH growing space activities, there is an increasing requirement to extend aerothermodynamic ground test facilities up to the superorbital regime. Typical examples of such activities are the STARDUST project run by NASA[1] and the MUSES-C project[2] run by the Institute of Space and Astronautical Science, Japan. For example, in the MUSES-C project, it is expected that the reentry capsule will experience the highest heat transfer at an altitude of 60 km and a speed of 12.5 km/s, which correspond to a stagnation enthalpy of about 70 MJ/kg. To optimize its heat shield design, quantitative on-ground experimental simulation is necessary.

There are several candidates among ground test facility types for such high-enthalpy flow experiments. A ballistic range is an ideal test facility because high-quality upstream conditions can be used at a room temperature level. However, with the current state of the art, with a reasonable model dimension it is extremely difficult to increase the flight speed up to this level. An arc jet is capable of attaining such a high enthalpy. However, it necessitates an expensive electrical power supply infrastructure. Moreover, it is difficult to suppress the maximum gas temperature that the test gas experiences before the process of steady-state expansion through a nozzle. This drawback often causes nonequilibrium states in the test flow. Free-piston shock tunnels have been used to study high-enthalpy flows. However, the test gas experiences a stagnation state during the process of enthalpy gain, leading to the problem of test flow contamination by melted nozzle material and by driver gas. Very high enthalpies (above 50 MJ/kg) are difficult to obtain.

An expansion tube[3,4] has unique characteristics as a high-enthalpy test device. In the process of generating high-enthalpy test flow, the test gas first experiences a shock compression, then unsteady expansion, and gains a total enthalpy. During the process of the unsteady expansion, the mechanical force originating in the pressure gradient results in an increase in the kinetic energy of the test gas while the static temperature is decreased. Therefore, the test gas does not experience such a high static temperature as is in reflected shock tunnels. The attainable stagnation enthalpy becomes higher than that with steady expansion.[4,5] Also, the possibility of material melting and resulting test-flow contamination, as often appears in reflected shock tunnels and arcjets, is much reduced.

Pioneering investigations on expansion tube operation were conducted at the NASA Langley Research Center.[6,7] They are currently continued by General Applied Science Laboratories.[8] Also, at the University of Queensland,[9–12] intensive experimental investigations have been conducted, exploring the possibility of a very-high-enthalpy regime. Morgan[5] experimentally proved that the expansion tube was practically capable of the simulation of superorbital high-enthalpy flows. Recently, Tohoku University has initiated an investigation on an expansion tube for the purpose of simulating superorbital flow over the MUSES-C reentry capsule.[13]

In a modest-size expansion tube, the test duration time is of the order of several tens of microseconds. Under a typical test condition of the present interest, p (pressure) $=4.1$ kPa, T (temperature) $=3800$ K, u (mass-averaged particle velocity) $=10$ km/s, δ/R (ratio of shock standoff distance to model radius) $=0.1$, and $R=40$ mm; the post-normal-shock conditions are calculated to be a (speed of sound) $=3.2$ km/s and $u=0.79$ km/s. Therefore, the characteristic time for a sound wave to propagate over a distance of 2δ is $2\delta/a=2.5$ μs; the characteristic time for convection is $\delta/u=5.1$ μs. At least around the stagnation region, quantitative aerothermodynamic simulation, including radiative heat transfer measurement and optical flow visualization, is possible even during this period. However, to date the feasibility of longer-term phenomena simulations like ablation from the heat shield is quite limited.

The interaction of super/hypersonic flow with gas injection from a blunt body has been attracting much interest among engineers, related not only to the ablating flow from reentry capsule heat shields but also to the improvement of aerodynamic characteristics.[14] If such simulation becomes feasible in expansion tubes under such high-enthalpy conditions, the usefulness of the device would become much improved. The purpose of this study is to develop an experimental system for high-enthalpy flow experiments with accompanying gas injection and to validate the effectiveness of the system.

II. Apparatus

Figure 1 schematically illustrates the superorbital expansion tube X-2 at the University of Queensland. The tube is composed of a two-stage, free-piston driver; a shock tube; an acceleration tube; and a test section. The total length of the facility is about 20 m. The inner diameter of the shock/acceleration tubes is 85 mm. The two-stage, free-piston driver is developed in order to achieve a high-enthalpy flow with reasonable facility dimensions.[5,15] At the

Received 1 April 1999; revision received 6 March 2000; accepted for publication 3 May 2000.

*Associate Professor, Shock Wave Research Center, Institute of Fluid Science, 2-1-1 Katahira, Aoba-ku. Associate Fellow AIAA.
†Associate Professor and Director, Center for Hypersonics, Department of Mechanical Engineering. Member AIAA.
‡Graduate Student, Department of Physics.
§Research Fellow, Department of Physics. Member AIAA.

end of the compression tube of the second-stage driver, a 2-mm-thick mild steel plate was inserted as the primary diaphragm. The fill pressures and species of the respective gases in the present study are indicated in Fig. 1. The generated freestream flow condition is tabulated in Table 1.

Figure 2 shows the schematic of the gas injection system. A reentry capsule model is set in the test section. A small amount of gas is injected from the stagnation region of the model. The injected gas is supplied by opening a solenoid valve. Under the nominal condition, the opening time of the valve is 20 ms, with a supplied step voltage of 24 V. To shorten its effective opening time, the peak voltage is increased to 100 V in absolute value. The solenoid valve is connected behind with a 6.4-mm-diam annealed copper tube, 6.8 m long in total. Hereafter, the fill pressure in the copper tube will be designated by p_0. The synchronization of the valve opening to the expansion tube operation is a critical issue in this study. The duration from the primary diaphragm rupture to the arrival of the test flow is about 1.1 ms, whereas the necessary duration for the solenoid valve opening is about 4 ms. Without proper synchronization the injected gas may increase the pressure in the acceleration tube, leading to the degradation of the test flow, or the gas injection does not become effective during the test period. In this study, the trigger signal to the solenoid valve opening is supplied on the basis of the static pressure measured 20 mm upstream from the end of the second-stage compression tube of the free-piston driver (Fig. 2). Further details on the synchronization will be described later. It is noted here that, if the gas is preinjected before the arrival of the test flow, the acceleration gas may be contaminated, whereas in principle the test gas, which is initially in the shock tube and is separated by a layer of diaphragm from the acceleration gas, is not contaminated.

Table 1 Freestream flow condition

Variable	Value
Pressure, kPa	4.1
Temperature, K	3800
Density, kg/m^3	3.1×10^{-3}
Stagnation enthalpy, MJ/kg	57
Flow Mach number	7.4
Dissociation fraction, N_2	0.013
Dissociation fraction, O_2	0.97

Figure 3a shows the design of the reentry capsule model with a single-hole injection. The pressure transducer and the shielding block to protect the solenoid valve against the high-enthalpy stream are also shown. The model is a $\frac{1}{10}$ scaled MUSES-C reentry capsule. Its blunt head is composed of a spherical tip of 40 mm in radius and a cone, the half-apex angle of which is 45 deg. The aft body is a 45-deg cone truncated at a 23.4-mm diam. The diameter of the gas passage becomes smallest (1.0 mm) at the exit. Immediately upstream from this location, an orifice of a smaller diameter (0.5 mm) can be inserted. In this paper, the smallest diameter of the passage is referred to as an "orifice diameter," whether or not the orifice piece is inserted. The static pressure upstream of the orifice is measured by a piezoresistive pressure transducer (Entran EPIS-080B-500). The pressure measured by this transducer is denoted by p_1. The shielding block is made of steel and is in the shape of a truncated wedge. The wedge angle (40 deg) is designed so that a shock wave over it is not detached under the test freestream condition. Figure 3b depicts another injector configuration: the gas is injected from the 0.75-mm-wide annular slit. The injection angle is about 120 deg from the mainstream direction.

Flow visualization is conducted by the schlieren method. The output of the Nd:YAG laser was frequency-doubled to provide a source of light with a wavelength of 532 nm. The output light has a spatial coherence and causes speckle on the schlieren image. To solve

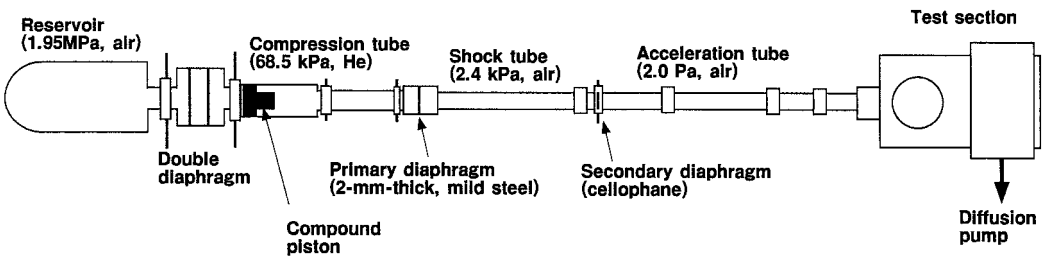

Fig. 1 Schematic illustration of the superorbital expansion tube X-2.

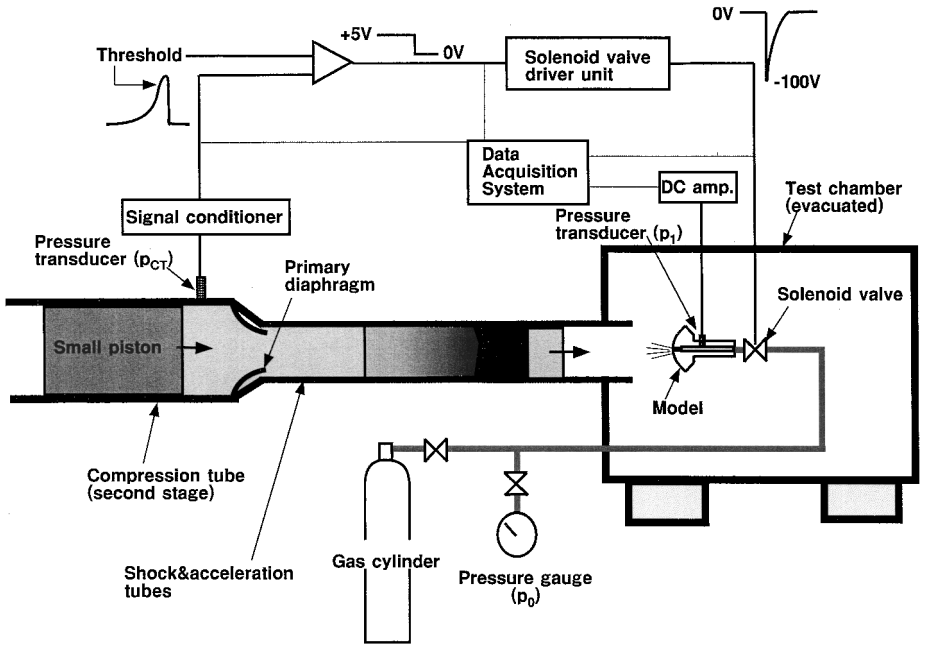

Fig. 2 Gas injection system as synchronized with the expansion tube operation.

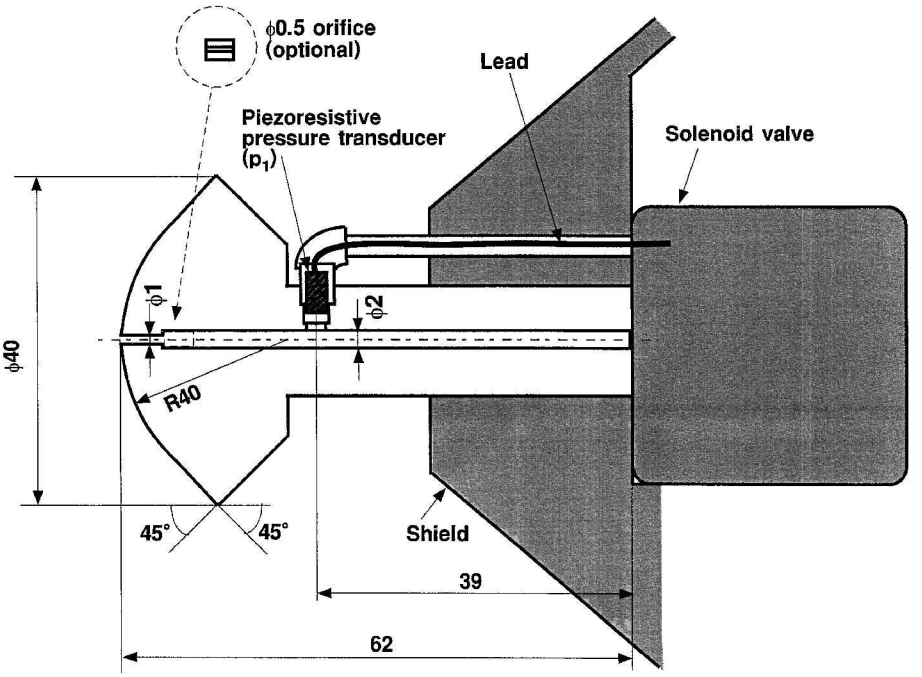

a) Model 1 (single-hole injection)

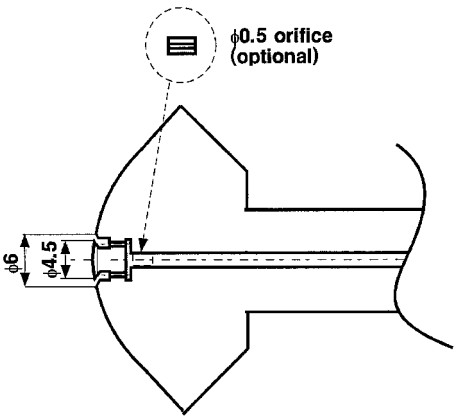

b) Model 2 (annular injection)

Fig. 3 Reentry capsule model, including a gas injector with a pressure transducer and shielding block.

this problem, the 532-nm light was introduced to a dye laser from which the front partial mirror had been removed, generating amplified spontaneous emission. The resulting beam of light had a central wavelength of 560 nm, with a full width at half-maximum of 20 nm. The exposure was synchronized to the expansion tube operation through a pressure signal measured in the shock tube. For the visualization, the laser was Q-switched, yielding an exposure time of 10 ns. The emission from the expansion tube gas flow was eliminated by a narrow-band optical filter and an aperture in front of the schlieren generating knife edge. This knife edge was set vertical. The schlieren image was recorded by a charge-coupled device camera (Kodak DCS410) that had 1524 × 1012 pixels.

III. Gas Injection Characteristics

A. Estimation of Mass Flow Rate

Measured time variations of p_1 with hydrogen injection through the 0.5-mm-diam orifice are shown in Fig. 4. The pressure varies almost as a pulse. Here a subscript 0 will denote an initial value in the copper feed tube. If p_0 is too high, the opening duration time and the pressure rise rate are decreased. This tendency appears in Fig. 4 for $p_0 = 795$ and 745 kPa. Except for these cases, both the opening pulse width and the pressure rise rate are almost constant. The pulse width is approximately 50 ms.

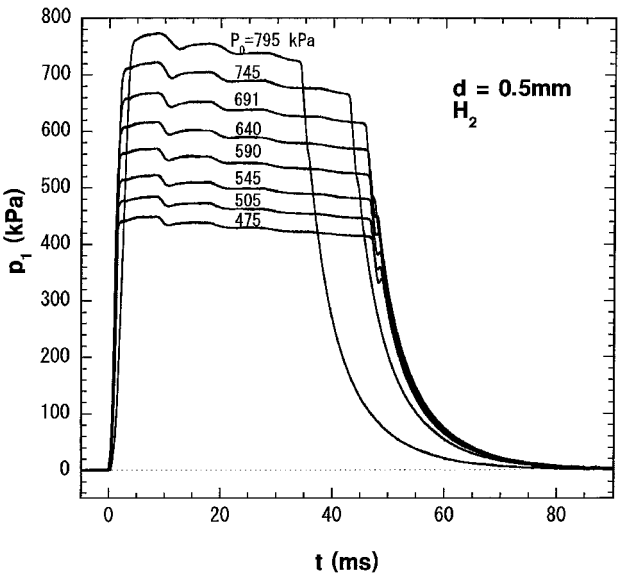

Fig. 4 Time variation of p_1 with hydrogen injection: orifice diameter = 0.5 mm.

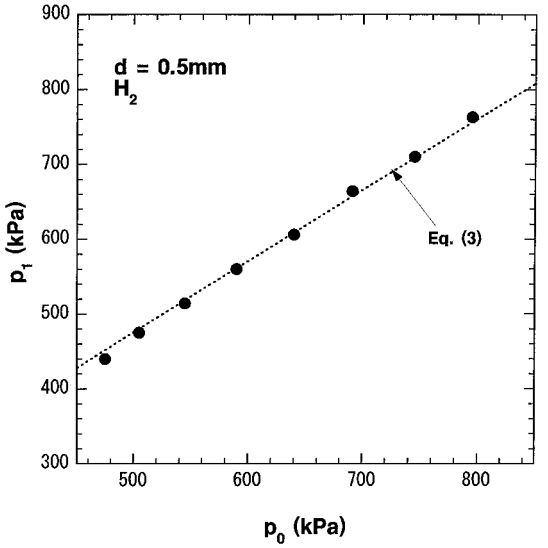

Fig. 5 Value p_1 vs p_0: ●, measured value, and - - - -, Eq. (3).

The effective value of p_1 is theoretically estimated in the following way: the valve is assumed to open instantaneously. Immediately after it opens, a quasi-steady-state flow is assumed to be established around the orifice. The flow is choked at the orifice. The flow Mach number upstream of the orifice, M_1, is implicitly given by the following one-dimensional flow relation for isentropic flow:

$$(A_1/A_*)^2 = \left(1/M_1^2\right)\left(2/(\gamma+1)\left\{1+[(\gamma-1)/2]M_1^2\right\}\right)^{(\gamma+1)/(\gamma-1)} \tag{1}$$

where A and γ designate the cross-sectional area and the specific heat ratio, respectively. The subscripts 1 and * correspond to values at the location 1, where the pressure transducer is mounted (Fig. 3a), and at the orifice, respectively. From the valve, expansion waves propagate upstream. Properties between 1 and 0 states are related by the conservation of a corresponding Riemann invariant. The mass flow rate $\dot{m}$ is estimated, together with Eq. (1), by

$$\dot{m} = \left(\frac{1+[(\gamma-1)/2]M_1^2}{[(\gamma+1)/2]\{1+[(\gamma-1)/2]M_1\}^2}\right)^{(\gamma+1)/2(\gamma-1)} \rho_0 a_0 A_* \tag{2}$$

where a and ρ designate the speed of sound and the density, respectively; p_1 is calculated by using the isentropic relation

$$p_1 = p_0\{1+[(\gamma-1)/2]M_1\}^{-2\gamma/(\gamma-1)} \tag{3}$$

Figure 5 shows by closed circles the measured relation between p_1 and p_0. With the orifice diameter of 0.5 mm, the deviation from Eq. (3) is ±2%. Therefore, the effective $\dot{m}$ can be reasonably estimated by Eq. (2). With the 1.0-mm-diam orifice (the result is not shown), however, the deviation becomes larger: ±9% at a maximum.

Figure 6 shows the time variations of p_1 normalized by p_0 measured with different orifice diameters and/or different gas species. With hydrogen injection the pressure rise time is approximately 2.0 ms, irrespective of the orifice diameter. With nitrogen injection, the pressure slowly rises over longer than 4.0 ms. This difference is caused by the difference in the speed of sound of the species. With hydrogen, the pressure waves propagate faster and the flow comes to a quasi-steady state more quickly.

B. Synchronization

As was briefly described in the Introduction, the necessary period from the trigger signal to the solenoid valve to the establishment of a quasi-steady-state gas injection is at least four times as long as the period during which an incident shock wave propagates through the shock tube and the acceleration tube. Therefore, the trigger signal needs to be supplied several milliseconds before the primary diaphragm rupture. The important condition for the synchronization of the gas injection to the test flow is high repeatability in timing of

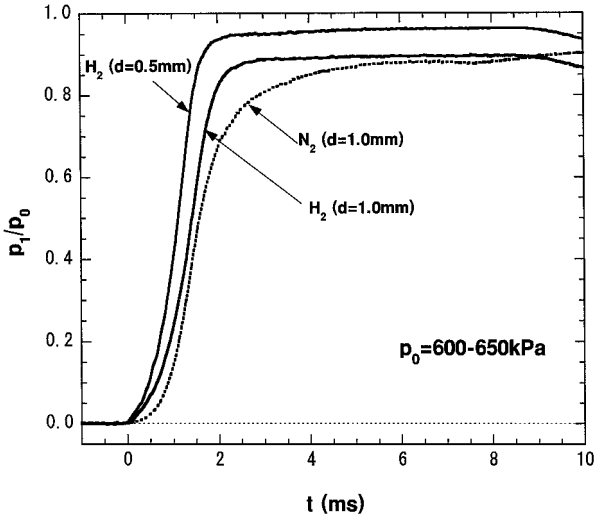

Fig. 6 Time variation of p_1, with different orifice diameters d and different species.

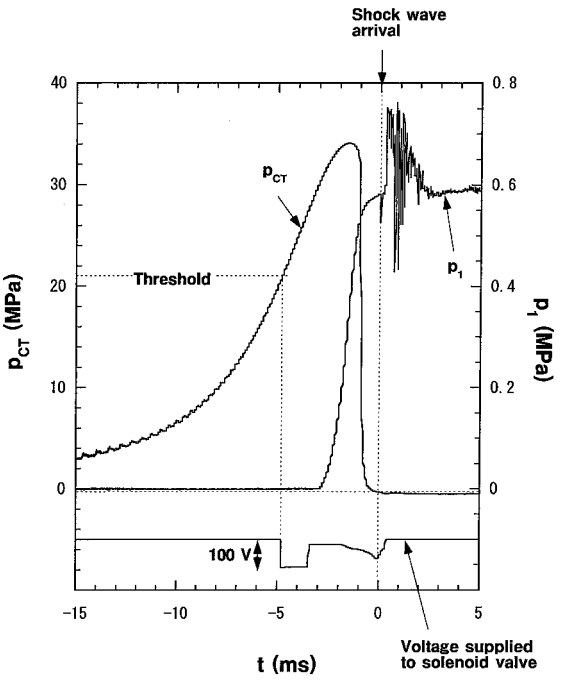

Fig. 7 Time variations of measured driver gas pressure p_{CT}, p_1, and the solenoid valve supply voltage; hydrogen injection, p_0 = 660 kPa; orifice diameter = 1.0 mm.

the trigger source signal. To minimize the scatter in the delay time, it is favorable that the trigger signal is originated by an event just before the primary diaphragm rupture. In the environment of the present study, the best solution for the trigger source was the pressure signal measured 20 mm upstream from the primary diaphragm in the second-stage compression tube.

Figure 7 shows the time variations of pressures related to the gas injection and of the valve supply voltage. Under the free-piston driver operation condition of the present study, the time variation of the pressure in the compression tube, p_{CT}, was found to be quite repeatable; the scatter in the peak pressure was ±3%, and that in the full time width of the half-maximum was about ±5%. The trigger timing to the solenoid valve opening was controlled by a threshold value of p_{CT}. With reasonable repeatability, the delay time could be varied by about 10 ms. At values of p_{CT} up to about 30 MPa, the rise rate of p_{CT} increases; hence, the uncertainty in the trigger timing is decreased by increasing the threshold value. As will be shown later, the injection of hydrogen had little effect on the shock wave propagation behavior in the acceleration tube.

As seen in Fig. 8, the pitot pressure under the present condition was measured to be about 240 kPa. The effective p_1 level is about 600 kPa, 2.5 times higher than the pitot pressure. Because of transient wave motions, as seen in Fig. 7, p_1 still fluctuates after the arrival of the incident shock wave at the test section. However, this event took place well after the test duration. Therefore, it is reasonably concluded that the gas was injected at an almost constant mass flow rate during the test period.

C. Effect on Acceleration Tube Performance

In Fig. 9, the x–t diagram of the incident shock wave through the shock tube and the acceleration tube with hydrogen injection at $p_0 = 600$ kPa is plotted with closed circles. The shock wave speed is calculated by taking the central derivative of the measured x–t relation and is plotted with open circles. The shock speed was about 5.0 km/s in the shock tube and 9.9 km/s in the acceleration tube. The shock speed variation without the gas injection is also plotted with squares. As seen in Fig. 9, the shock speed near the exit of the acceleration tube was not affected by the hydrogen injection. The trigger signal to the solenoid valve was supplied 6.5 ms before the

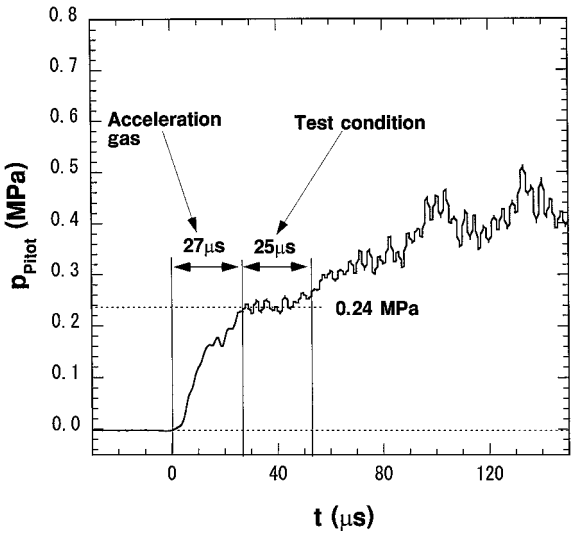

Fig. 8 Time variation of pitot pressure measured on the centerline at the test section.

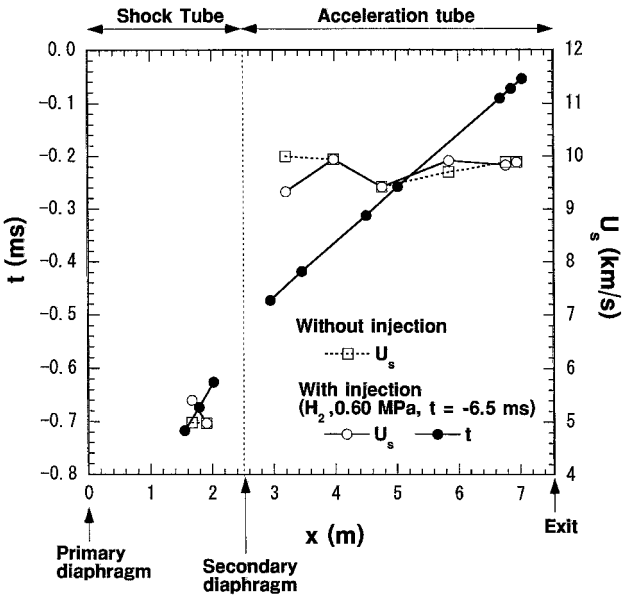

Fig. 9 An x–t diagram of incident shock wave propagation and spatial variations of the shock wave speed: ○, ●, with hydrogen injection; and □, without injection. Trigger signal to the solenoid valve was supplied at $t = -6.5$ ms. $t = 0$ corresponds to the arrival of the shock wave at the exit of the acceleration tube. Orifice diameter = 1.0 mm.

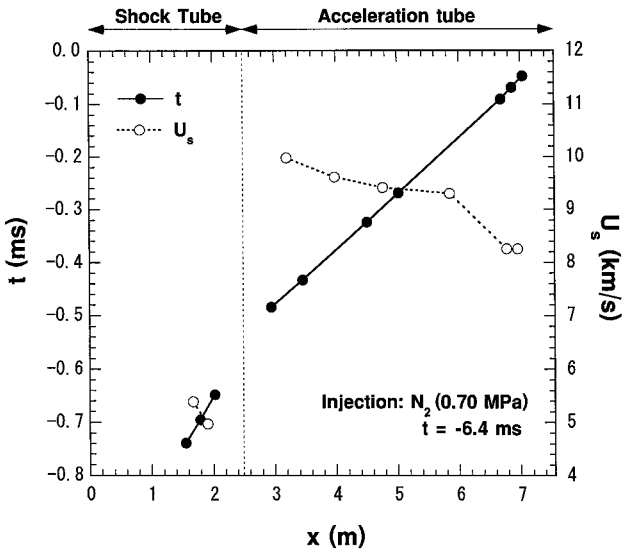

Fig. 10 An x–t diagram of incident shock wave propagation and spatial variations of the shock wave speed with nitrogen injection. Trigger signal to the solenoid valve was supplied at $t = -6.4$ ms. $t = 0$ corresponds to the arrival of the shock wave at the exit of the acceleration tube. Orifice diameter = 1.0 mm.

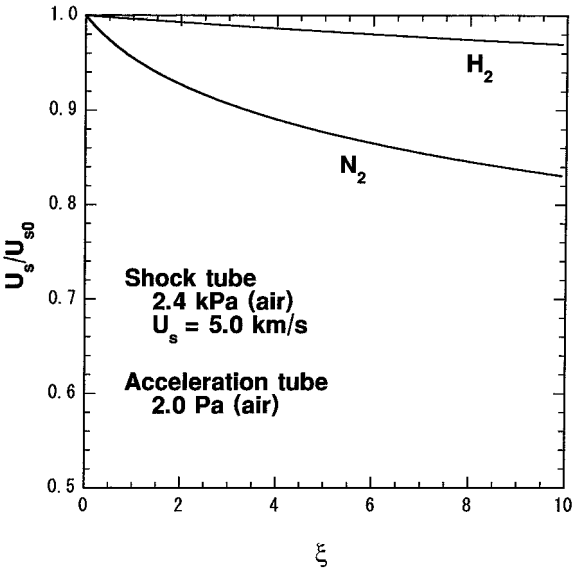

Fig. 11 Effect of fraction of injected gas on the shock wave speed in the acceleration tube, calculated for calorically perfect gas: ξ, mole ratio of injected gas to ambient air; U_s, shock speed; and U_{s0}, shock speed with $\xi = 0$.

arrival of the incident shock wave at the exit of the acceleration tube. In the case shown in Fig. 7, the trigger signal was supplied 4.8 ms before the arrival. This implies that in the case shown in Fig. 9, even 1.7 ms after establishing a quasi-steady-state injection condition the hydrogen injection did not affect the shock speed. However, when nitrogen was injected under a similar condition, the shock wave speed was decreased by 17% (Fig. 10).

This difference between the species is explained by considering the change in the properties of the acceleration gas. Figure 11 shows the calculated dependence of the shock wave speed in the acceleration tube on the mole concentration ratio ξ of the injected gas to the ambient air initially filled in the acceleration tube. This calculation is done under the same initial condition in the shock tube and the acceleration tube as in the present experiment. The gases are assumed to be calorically perfect. The shock speed in the shock tube is assumed to be 5.0 km/s. The operation condition is determined from pressure/particle velocity matching at the contact surface. Under the injection condition shown in Fig. 9, if the

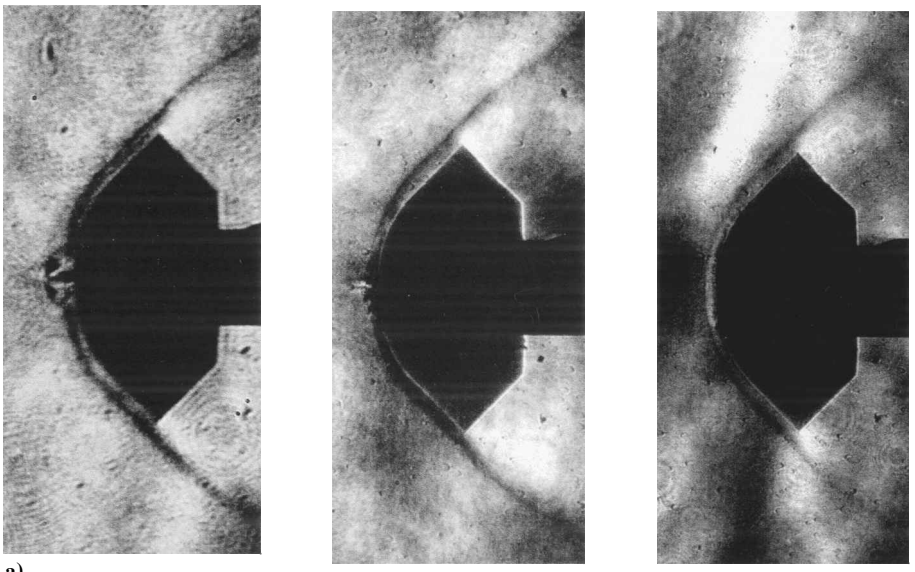

Fig. 12 Schlieren images of the hypersonic bow shock wave with hydrogen injection: a) $p_0 = 600$ kPa, orifice diameter = 1.0 mm; solenoid valve trigger: $t = -6.5$ ms (model 1); b) $p_0 = 630$ kPa, orifice diameter = 0.5 mm; solenoid valve trigger: $t = -7.1$ ms (model 1); and c) $p_0 = 650$ kPa, orifice diameter = 1.0 mm; solenoid valve trigger: $t = -3.4$ ms (model 2).

injected gas is uniformly distributed in the acceleration tube and the test section, ξ is estimated to be 0.67. As seen in Fig. 11, the shock speed is decreased only by 0.3%. It is expected that, because the gas was injected directly toward the acceleration tube, the real hydrogen fraction was higher in the acceleration tube. By increasing the amount of hydrogen injection, the molecular mass of the mixture is decreased, compensating for the increase in the static pressure. As a result, U_s is insensitive to ξ with the hydrogen injection in a wide ξ range. As seen in Fig. 11, U_s is decreased only 3%, even for $\xi = 10$.

If nitrogen is injected, however, the pressure of the mixture almost linearly increases with ξ, not being accompanied by a significant decrease in molecular mass. The performance of the acceleration tube operation is much degraded. In Fig. 11, with nitrogen injection of $\xi = 10$, U_s is decreased by 17%. This simple analysis well explains the measured shock speed dependency on the gas species injected. It follows from these results that only with the hydrogen injection is the high-enthalpy generation performance not degraded in the present experiment.

IV. Flow Visualization

Figure 8 shows the time variation of the pitot pressure measured without gas injection to the test section. The pitot pressure gradually rises for about 27 μs. This duration roughly corresponds to the passage of the acceleration gas. After this transient period, the test flow arrives and the pitot pressure becomes almost constant at about 240 kPa. This test duration lasts for about 25 μs. The exposure of the laser light for the flow visualization needs to be done during this period.

Figure 12 is composed of three schlieren images of the test flow with hydrogen injection. Although the quality of the images could be improved, it is sufficient for demonstrating the effectiveness of this gas injection system. As shown by Fig. 12a, hydrogen is injected through the 1-mm-diam orifice with $p_0 = 600$ kPa. In this case, the dynamic pressure of the injected hydrogen is so high that the bow shock wave is pushed forward by the injected gas. A ring vortex is observed around the tip of the penetrating jet.

In the case of Fig. 12b, the orifice diameter is decreased to 0.5 mm. Downstream of the orifice in the injection passage, the hydrogen flows through the 1.0-mm-diam passage. It was expected that in this passage a normal shock wave is generated and the dynamic pressure of the hydrogen jet is decreased to better match to the postshock pressure. As seen in Fig. 12b, the bow shock was not so much disturbed as in the previous example. However, there still is observed a thin hydrogen jet along the stagnation line.

In these two cases, the injector configuration of model 1 is used. When p_0 was much decreased, the injected gas was not observed due to the lower supply pressure. To get better matching between the postshock pressure and the gas injection, the annular injector configuration of model 2 (Fig. 3b) was tested. The intention of this injector shape was to suppress the dynamic pressure of the jet by increasing the cross-sectional area of the flow passage and by putting an obstacle against direct injection toward the upstream direction. Figure 12c is a schlieren image taken with this annular injector. The shape of the bow shock wave in this case is not disturbed. Around the stagnation point in the shock layer, a distinct bright region appears. This is believed to be a stagnating hydrogen bubble. Under an equal pressure, the refraction sensitivity of hydrogen is about half as large as that of air. Therefore, a high hydrogen concentration under a uniform pressure takes the same role as a density decrease. However, from this image alone it is difficult to see detailed flow pattern of the injected hydrogen. Depending on a specific application of the system, the modification of the injector design warrants further investigation.

V. Conclusions

In the present study, it is experimentally shown that hypersonic flow with gas injection is possible by using the superorbital expansion tube. In particular, if hydrogen is injected, the performance of the acceleration tube is not degraded, even with a large amount of injection. It is expected that by using this system, superorbital flow with ablation can be simulated by injecting hydrogen from the surface of a model. For conducting more practical simulations, a modification of the injector design, including the employment of porous material to the wall surface, warrants further investigation. An independent work on radiative and convective heat transfer measurement will be combined with the present work to produce quantitative simulation of superorbital flows.

Acknowledgments

The authors thank Paul Siegrist, an undergraduate student in the Department of Mechanical Engineering, University of Queensland, for valuable help in conducting this experiment. Technical assistance from the mechanical and electrical workshops of the same department is greatly appreciated.

References

[1] Gupta, R. N., "Aerothermodynamic Analysis of Stardust Sample Return Capsule with Coupled Radiation and Ablation," AIAA Paper 99-0227, Jan. 1999.

[2]Suzuki, K., Kubota, H., Fujita, K., and Abe, T., "Chemical Nonequilibrium Ablation Analysis of MUSES-C Super-Orbital Reentry Capsule," AIAA Paper 97-2481, June 1997.

[3]Resler, E. L., and Blossom, D. E., "Very High Mach Number Flows by Unsteady Flow Principles," Cornell Graduate School of Aerospace Engineering Monograph, Cornell Univ., Ithaca, NY, 1952.

[4]Trimpi, R. L., "A Preliminary Technical Study of the Expansion Tube, A New Device for Producing High-Enthalpy Short-Duration Hypersonic Gas Flows," NASA Rept. R-133, 1962.

[5]Morgan, R. G., "Superorbital Expansion Tube," *Proceedings of 21st International Symposium on Shock Waves*, Vol. 1, Panther, Canberra, Australia, 1997, pp. 71–76.

[6]Miller, C. G., "Flow Properties in Expansion Tube with Helium, Argon, Air, and CO_2," *AIAA Journal*, Vol. 12, No. 4, 1974, pp. 564–566.

[7]Miller, C. G., "Operation Experience in the Langley Expansion Tube with Various Test Gases," *AIAA Journal*, Vol. 16, No. 3, 1978, pp. 195, 196.

[8]Calleja, J., and Tamagno, J., "Calibration of HYPULSE for Hypervelocity Air Flows Corresponding to Flight Mach Numbers 13.5, 15 and 17," NASA CR-191578, Dec. 1993.

[9]Neely, A. J., Stalker, R. J., and Paull, A., "High Enthalpy Hypervelocity Flows of Air and Argon in an Expansion Tube," *Aeronautical Journal*, Vol. 95, No. 946, 1991, pp. 175–186.

[10]Paull, A., and Stalker, R. J., "Test Flow Disturbances in an Expansion Tube," *Journal of Fluid Mechanics*, Vol. 245, 1992, pp. 493–521.

[11]Neely, A. J., and Morgan, R. G., "The Superorbital Expansion Tube Concept, Experiment and Analysis," *Aeronautical Journal*, Vol. 98, No. 973, 1994, pp. 97–105.

[12]Bakos, R. J., and Morgan, R. G., "Chemical Recombination in an Expansion Tube," *AIAA Journal*, Vol. 32, No. 6, 1994, pp. 1316–1319.

[13]Sasoh, A., Ohnishi, Y., Koremoto, K., and Takayama, K., "Generation of High Enthalpy Flows Using a Free-Piston-Driven Expansion Tube," *Proceedings of 21st International Symposium on Space Technology and Science*, Vol. 1, Sanbi-Insatsu, Tokyo, 1998, pp. 881–886.

[14]Ganiev, Y. C., Gordeev, V. P., Krasilnikov, A. V., Lagutin, V. I., Otmennikov, V. N., and Panasenko, A. V., "Aerodynamic Drag Reduction by Plasma and Hot-Gas Injection," *Journal of Thermophysics and Heat Transfer*, Vol. 14, No. 1, 2000, pp. 10–17.

[15]Doolan, C. J., and Morgan, R. G., "A Two Stage Free-Piston Driver for Expansion Tubes," AIAA Paper 96-0854, Jan. 1996.

M. Sichel
Associate Editor